

1 **Pre-print**

2 Marco G. Malusà, Liang Zhao, Elena Eva, Stefano Solarino, Anne Paul,  
3 Stéphane Guillot, Stéphane Schwartz, Thierry Dumont, Coralie Aubert, Simone  
4 Salimbeni, Silvia Pondrelli, Qingchen Wang & Rixiang Zhu

5 **Earthquakes in the western Alpine mantle wedge**

6 Gondwana Research, 2017, 44: 89-95

7 *<http://dx.doi.org/10.1016/j.gr.2016.11.012>*

8

# 9 Earthquakes in the western Alpine mantle wedge

10 <http://dx.doi.org/10.1016/j.gr.2016.11.012>

11 Marco G. Malusà<sup>1\*</sup>, Liang Zhao<sup>2</sup>, Elena Eva<sup>3</sup>, Stefano Solarino<sup>3</sup>, Anne Paul<sup>4</sup>, Stéphane  
12 Guillot<sup>4</sup>, Stéphane Schwartz<sup>4</sup>, Thierry Dumont<sup>4</sup>, Coralie Aubert<sup>4</sup>, Simone Salimbeni<sup>5</sup>, Silvia  
13 Pondrelli<sup>5</sup>, Qingchen Wang<sup>2</sup> & Rixiang Zhu<sup>2</sup>

14 <sup>1</sup> *Department of Earth and Environmental Sciences, University of Milano-Bicocca, Piazza della Scienza 4, 20126*  
15 *Milano, Italy.*

16 <sup>2</sup> *State Key Laboratory of Lithospheric Evolution, Institute of Geology and Geophysics, Chinese Academy of*  
17 *Sciences, Beijing, China.*

18 <sup>3</sup> *Istituto Nazionale di Geofisica e Vulcanologia, CNT, Genova, Italy.*

19 <sup>4</sup> *ISTerre, CNRS, Université Grenoble Alpes, Grenoble, France.*

20 <sup>5</sup> *Istituto Nazionale di Geofisica e Vulcanologia, Bologna, Italy.*

21 *\* Corresponding author (email: marco.malusa@unimib.it)*

## 22 **Abstract**

23 The assessment of seismic activity in the shallow continental mantle has long been  
24 hindered by the low resolution of both seismic imaging and earthquake locations in young  
25 collision zones. Here, we combine the most recent and high-resolution image of the  
26 lithospheric structure of the Western Alps with a high quality dataset of anomalously deep  
27 earthquakes recorded in the same area in the past 25 yrs. We show that these earthquakes are  
28 aligned on an active lithospheric strike-slip fault, and we provide evidence that this fault is  
29 located in the mantle wedge beneath the Adriatic Moho. Our results: (i) provide direct  
30 evidence that deep material can be seismogenic or not depending on the lithology; (ii) confirm  
31 the role of serpentinization in favoring the aseismic creep of mantle rocks; and (iii)  
32 demonstrate that the upper mantle can be stiff and seismogenic not only in cold cratons, but  
33 also in young orogenic belts.

34 **Keywords:** deep Alpine structure; mantle earthquakes; focal mechanism heterogeneity;  
35 aseismic creep; lithosphere rheology.

36

## 37 **1. Introduction**

38 The mechanical properties of the continental upper mantle are very important for the  
39 interpretation of lithospheric processes at all time and spatial scales (Richards et al., 2001;  
40 Bürgmann and Dresen, 2008), but in spite of the relevant implications, these properties are  
41 still highly debated (Chen and Molnar, 1983; Jackson, 2002; Burov and Watts, 2006;  
42 Monsalve et al., 2006; Priestley et al., 2008; Chen et al., 2013). A strong and rigid mantle may  
43 explain the topographic stability of mountain belts and the slab integrity during subduction  
44 (Burov and Watts, 2006; Mouthereau et al., 2013), while the shallow depth of most  
45 continental earthquakes may instead suggest that the long-term strength of the continental  
46 lithosphere resides in the crust (Maggi et al., 2000a; Jackson, 2002). So far, evidence of  
47 seismic activity and brittle faulting in the continental mantle has limited spatial coverage  
48 (Chen and Molnar, 1983; Maggi et al., 2000b; Monsalve et al., 2006; Priestley et al., 2008;  
49 Frohlich et al., 2015; Inbal et al., 2016) and the loci of deep earthquakes are often poorly  
50 constrained relative to nearby plate interfaces (Negredo et al., 2007; Priestley et al., 2008;  
51 Kufner et al., 2016). In the field, some xenoliths of mantle rocks show brittle cataclastic  
52 textures (Takeuchi and Arai, 2015) and pseudotachylytes do occur in outcrops of mantle  
53 peridotite (Andersen and Austrheim, 2006), yet most exhumed mantle slivers bear sole  
54 evidence of high-temperature ductile shear (Vauchez et al., 2012).

55 Here, we shed light on this issue by combining the most recent high-resolution image of  
56 the lithospheric structure of the Western Alps with a high quality dataset of anomalously deep  
57 earthquakes recorded in the same area during the past 25 yrs. Our results provide new

58 constraints on mantle rheology along convergent plate boundaries, and have major  
59 implications for a wide range of studies, from the local scale to large scale geodynamics.

60

## 61 **2. The Western Alps study area**

62 The Western Alps are the result of the Cretaceous-to-Paleogene oblique subduction of the  
63 European plate beneath the Adriatic microplate (Jolivet et al., 2003; Handy et al., 2010;  
64 Malusà et al., 2015). They include a thick subduction complex, now exhumed at the surface  
65 (Lardeaux et al., 2006; Malusà et al., 2011), and they are seismically active despite  
66 subduction ceased more than 30 Myrs ago (Eva and Solarino, 1998; Delacou et al., 2004).  
67 During the collision stage, deformation propagated towards the European foreland (Dumont et  
68 al., 2012; Bellahsen et al., 2014), and GPS measurements attest that Adria-Europe  
69 convergence is now chiefly accommodated outside the Western Alps accretionary wedge  
70 (e.g., Serpelloni et al., 2005).

71 Seismicity in the Western Alps typically shows low to moderate energy ( $2 < M < 4$   
72 magnitude), and is usually confined within the upper crust (Eva et al., 1997; Eva and Solarino,  
73 1998; Sue et al., 1999; Perrone et al., 2010), but hundreds of anomalously deep earthquakes  
74 have been also recorded on the upper plate side of the orogenic belt, along the boundary with  
75 the Po Plain (Eva et al., 2015). However, the low resolution of earthquake locations, and the  
76 lack of high-resolution images of the Western Alps lithospheric structure, have long  
77 precluded a reliable positioning of these earthquakes relative to the plate interface, hindering  
78 any further step in the investigation of the rheological properties of the continental lithosphere  
79 in the study area.

80 In order to shed light on this issue, the whole earthquake dataset was recently reprocessed  
81 by Eva et al. (2015) to improve earthquake locations, whereas new constraints on the  
82 lithospheric structure were provided by the passive seismic experiment CIFALPS (China-

83 Italy-France Alps Seismic survey) using the P-receiver-function technique (Zhao et al., 2015).  
84 These two datasets are combined here for the first time.

85 Noteworthy, the linear transect defined by the CIFALPS temporary broadband seismic  
86 stations is located just in correspondence of the main cluster of anomalously deep earthquakes  
87 (Fig. 1). This was particularly important in the light of the complex 3D structure expected in  
88 the Western Alps, where Adria-Europe convergence was strongly oblique relative to the  
89 orogen trend during most of the Cenozoic (Dewey et al., 1989; Jolivet et al., 2003), and  
90 deformation during subduction and collision was strongly partitioned across the orogen  
91 (Malusà et al., 2009; 2015).

92

### 93 **3. Methods**

94 The methods employed for earthquake analysis and seismic imaging are described in full  
95 in Eva et al. (2015) and Zhao et al. (2015), and are summarized here to underline the  
96 reliability of the datasets employed in this work. We considered the anomalously deep  
97 earthquakes (depth > 20 km) recorded from 1990 to 2014 within the quadrangle 44°00'N –  
98 45°30'N and 6°30'E – 8°30'E. The network used to record the seismicity (red triangles in Fig.  
99 1) includes stations from RSN INGV Roma, SISMALP Grenoble Observatory, OCA  
100 GeoAzur Nice and SED-ETH Zürich. Data were selected according to the number of phase  
101 readings (at least 8 P+S), which led to a dataset of 590 earthquakes and ~12,500 three-  
102 component waveforms, equally distributed between P- and S-wave pickings. Seismograms  
103 were revised by a complete manual phase picking. We applied to the dataset the double  
104 difference relocation technique (HypoDD) (Waldhauser and Ellsworth, 2000). Cross-  
105 correlations were computed for stations at <100 km distance from the center of the selected  
106 area, whereas stations at >100 km distance were additionally considered for catalogue data.

107 We thus obtained ~25,000 cross correlation difference times to use in the computation with  
108 HypoDD, complemented by ~780,000 catalogue differential times.

109 Fault plane solutions were computed by E.E. for relocated events with magnitude >2.6  
110 MI, according to the first onset technique and using the FPFIT software (Reasenberg and  
111 Oppenheimer, 1985). We selected earthquakes having at least 15 readable, evenly distributed  
112 polarities (gap <110°), using for computation the output hypocentral parameters obtained with  
113 HypoDD.

114 The location of the temporary broadband seismic stations of the CIFALPS passive  
115 seismic experiment, which operated from July 2012 to September 2013, is shown in Figure 1.  
116 Their spacing ranges from 5 km in the mountain belt to 10 km in the Po Plain, where specific  
117 problems related to anthropogenic noise and unconsolidated sediments were minimized by  
118 selecting sites in outcrops of Oligo-Miocene sedimentary rocks exposed atop the Monferrato  
119 thrust fronts (Fig. 1). Events with magnitude  $\geq 5.5$  and epicentral distance from 30° to 90°  
120 were selected for calculation of the receiver functions. Three-component recordings of distant  
121 earthquakes were band-pass filtered and rotated into the local coordinate system. We  
122 excluded P-wave records with signal-to-noise ratio <2 on the radial component, and removed  
123 the remaining low-quality records by visual inspection. After computing radial and transverse  
124 receiver functions according to the method described in Ligorria and Ammon (1999), we  
125 performed a second round of visual inspections to remove low-quality receiver functions. As  
126 a result, we obtained a dataset of 1,647 radial receiver functions from 84 events.

127 To produce a depth image beneath the receiver array, we migrated the time data to depth,  
128 and stacked the radial receiver functions using the common conversion point (CCP) method  
129 (Zhu, 2000). We used the resulting depth section and other geophysical and geologic  
130 constraints to define the geometry of possible 2D models and the main layer boundaries and  
131 velocity contrasts (Zhao et al., 2015). After constructing the model geometry, we checked its

132 compatibility with the Bouguer anomaly data by gravity modeling, and performed 2D  
133 synthetic tests in order to test the interpretation of the CCP section that fits the Bouguer  
134 anomaly data.

135

#### 136 **4. Earthquake distribution**

137 The 317 events out of 590 recorded in the Western Alps at depth >20 km, and  
138 successfully relocated with the HypoDD algorithm, are distributed within a roughly N-S  
139 trending belt in map view (Fig. 1). These anomalously deep earthquakes show, in 90% of the  
140 cases, both horizontal and vertical location errors <2.5 km, and their epicenters define three  
141 clusters. The main linear cluster (1, purple in Fig. 1), recently referred to as the Rivoli-Marene  
142 deep fault (Eva et al., 2015), is located beneath the Western Po Plain, and includes the highest  
143 magnitude events, with depth constrained between 25 and 75 km. In cross section, these  
144 events define an apparent plane steeply dipping towards ENE (Fig. 2a). Minor clusters of  
145 lower magnitude events, with depth constrained between 20 and 40 km, are found on the  
146 southeastern margin of the Dora-Maira massif (2 in Fig. 1), and north of the Monferrato thrust  
147 front (3 in Fig. 1). No anomalously deep earthquake is found farther north, possibly due to a  
148 change in tectonic boundary conditions (Malusà et al., 2009; 2015). Fault plane solutions  
149 invariably show a strike-slip component (see beach balls in Fig. 1), which contrasts with the  
150 dominant extensional solutions associated with earthquakes shallower than 20 km (e.g., Eva  
151 and Solarino, 1998; Sue et al., 1999). Along the analyzed cross section, the 30-50 km depth  
152 earthquakes show compressive to transpressive solutions, whereas the 50-80 km depth  
153 earthquakes show strike-slip solutions with a slight compressive component (Fig. 2b). Fault  
154 plane solutions thus depict an heterogeneity of focal mechanisms with a stacking of  
155 extensional, compressional and strike-slip events as a function of depth (Fig. 3a), that will be  
156 discussed in more detail in section 6.1.

157

## 158 **5. Lithospheric structure**

159 The lithospheric structure imaged by the P-receiver-function technique is shown in Figure  
160 2a, whereas the corresponding 2D velocity and gravity model is shown in Figure 2b. The P-  
161 receiver-function technique enhances P-to-S (Ps)-converted waves on velocity interfaces  
162 beneath an array in the records of teleseismic earthquakes. The polarity of the converted  
163 signal depends on the sign of the velocity change, which allows for an easy discrimination  
164 between interfaces with velocity increase (red-to-yellow in Fig. 2a) and interfaces with  
165 velocity decrease (blue in Fig. 2a). Our seismic experiment imaged two major interfaces with  
166 velocity increase, corresponding to the European and Adriatic Mohos already imaged by  
167 previous work (e.g., Thouvenot et al., 2007; Molinari et al., 2015), and a major interface with  
168 velocity decrease. The European Moho is continuously marked by Ps-conversions with  
169 positive polarity, dipping towards the east from ~40 km depth beneath the Frontal Pennine  
170 Fault to ~75 km depth beneath the westernmost Po Plain. The weakening of this converted  
171 phase beneath the accretionary wedge may be due to eclogitization, and consequent density  
172 increases with metamorphic phase changes, of the European lower crust at depth >40 km. The  
173 European Moho is not imaged by the P-receiver-function technique at depth >75 km.  
174 However, it is expected to become steeper below 75 km depth, in the light of the attitude of  
175 the European slab inferred from P-wave tomography constraints (e.g., Piromallo and  
176 Faccenna, 2004; Zhao et al., 2016).

177 The Adriatic Moho imaged by our receiver function analysis is marked, in Fig. 2a, by  
178 shallower positive-polarity Ps-conversions, recognized at 20-30 km depth to the east and 10-  
179 15 km depth to the west. In the westernmost Po Plain, this interface coincides with the top of  
180 the so-called 'Ivrea body' (Closs and Labrouste, 1963), classically interpreted as a southward-  
181 plunging slice of Adriatic mantle at shallow crustal depth (Nicolas et al., 1990; Scafidi et al.,



182 2009). Synthetic tests show that the underlying red spots located at 40-55 km depth (see Fig.  
183 2a) are instead multiples (Zhao et al., 2015). A shallow positive-polarity converted phase is  
184 also observed beneath the Dora-Maira massif, and it is interpreted to mark a downward  
185 velocity increase from (ultra)high-pressure [(U)HP] crustal rocks to mantle rocks underneath  
186 (Fig. 2b). The main negative polarity conversions (thick blue spot in Fig. 2a) recognized at  
187 20-40 km depth beneath the Dora-Maira massif, may mark instead a downward velocity  
188 decrease from mantle rocks to (U)HP slivers of European crust and associated serpentinites of  
189 the suture zone (Fig. 2b). Two end-member tectonic reconstructions, both consistent with  
190 geophysical data (Zhao et al., 2015) are shown in Fig. 3, and will be used to discuss the  
191 relationships between seismicity and lithospheric structure in section 6. In figure 3a, the  
192 downward velocity decrease revealed by the CIFALPS experiment is entirely ascribed to a  
193 thick complex of (U)HP continental slivers, in line with the predictions of recent numerical  
194 models of synconvergent exhumation (e.g., Jamieson and Beaumont, 2013). In figure 3b,  
195 instead, the downward velocity decrease is entirely ascribed to the serpentinitization of the  
196 mantle wedge on top of the slab, with a larger volume of mantle involved that may be  
197 expected, for instance, in the case of exhumation triggered by divergence between upper plate  
198 and accretionary prism (e.g., Malusà et al., 2015). Discriminating between these end-member  
199 models is beyond the aim of this work. Both (U)HP continental slivers and serpentinites may  
200 be found in correspondence of the thick blue spot of negative polarity conversions shown in  
201 Fig. 2a, but the relative proportion of these rocks cannot be assessed on the basis of available  
202 geophysical constraints, and would require further investigations.

203

## 204 **6. Discussion**

### 205 **6.1. Earthquakes in the continental mantle**

206       When the earthquakes relocated with HypoDD are plotted on the new lithospheric image  
207 provided by the CIFALPS experiment (Fig. 2), it is clear that the shallow earthquakes (<20  
208 km depth) (e.g., Eva and Solarino, 1998; Sue et al., 1999) are concentrated within the uplifting  
209 accretionary wedge (Serpelloni et al., 2013), i.e., between the Frontal Pennine Fault and the  
210 Dora Maira massif (DM in Fig. 2a). By contrast, no diffuse shallow seismicity is observed  
211 farther east in the subsiding Po Plain, where shallow events are clustered along few main  
212 tectonic structures such as the Villalvernia-Varzi Fault (e.g., Malusà and Balestrieri, 2012).  
213 This confirms that extensional faulting during rock uplift plays a major role in controlling the  
214 shallow seismicity of the Western Alps (Eva and Solarino, 1998; Sue et al., 1999).

215       But the most intriguing information provided by Fig. 2 is that the anomalously deep  
216 earthquakes of the Western Alps are located well below the Adriatic Moho. Events deeper  
217 than 20 km, and located within the 40-km-thick stripe of Figure 1, probably originated either  
218 within the Adriatic mantle beneath the Po Plain, or within the mantle sandwiched between the  
219 Dora Maira (U)HP rocks and the (U)HP metamorphic slivers and/or the serpentized mantle  
220 of the suture zone underneath (Fig. 2b). No deep seismicity is instead observed along the  
221 imaged European Moho or its continuation at depth, as expected since subduction is no more  
222 active. The earthquakes located below the Adriatic Moho define two main alignments with  
223 different dip angles (“a” and “b” in Fig. 2a). The alignment “a” dips at low angle towards the  
224 east, and is parallel to the main interface with downward velocity decrease imaged beneath  
225 the Dora Maira massif (Fig. 2b). Noteworthy, most of the events ascribed to the alignment “a”  
226 lay within the mantle above this interface, and only few events are located within the (U)HP  
227 continental slivers (Fig. 3a) or the serpentized mantle (Fig. 3b) underneath. The alignment  
228 “b” dips instead at high angle towards the east, and marks an active sinistral lithospheric fault  
229 that crosscuts the whole mantle suture zone between the Adriatic Moho and the European  
230 Moho. This fault accommodated the post-Oligocene differential motion between the Adriatic

231 lithosphere and the Alpine wedge on top of the European slab, locally juxtaposing crustal  
232 rocks against mantle rocks. Outside of the main alignment “b”, earthquakes predominantly lay  
233 within the Adriatic mantle east of the fault, whereas only few events lay within the continental  
234 crust and/or the serpentized mantle to the west of the fault.

235       The heterogeneity of focal mechanisms with depth observed below the Adriatic Moho  
236 may be explained with strain partitioning along pre-existing tectonic structures. In the depth  
237 range from 30 to 50 km, seismic events have oblique focal mechanisms and a less important  
238 strike–slip component compared to the events deeper than 50 km. At 30-50 km depth, the  
239 receiver-function cross-section also highlights a vertical change in lithospheric structure,  
240 which is dominated by the shallow dipping contact between mantle rocks not affected by  
241 serpentization on top, and the (U)HP continental slivers and/or serpentized mantle rocks  
242 below (Fig. 2b). This suggests that the anomalously deep earthquakes with oblique and strike-  
243 slip focal mechanisms could be a response to the same global stress field controlled by the  
244 ongoing convergence between Africa and Europe, but accommodated along shallow dipping  
245 and steeply dipping pre-existing faults, respectively, at different depths within the lithosphere  
246 (Jolivet et al., 2003; Serpelloni et al., 2005). The Western Alps are oriented near-parallel to  
247 present-day Adria motion relative to stable Europe (Serpelloni et al., 2005), which explains  
248 the importance of strike-slip deformation along this segment of the Adria-Europe plate  
249 boundary.

250       Previous work suggested the occurrence of earthquakes at shallow mantle depth (Chen  
251 and Molnar, 1983; Chen and Yang, 2004; Monsalve et al., 2006), but the mantle origin of  
252 those earthquakes was not proven (Maggi et al., 2000b; Priestley et al., 2008). The locations  
253 of the anomalously deep earthquakes of the Western Alps have been progressively confirmed  
254 by improved techniques over 25 years of continuous recording (Eva et al., 2015). By  
255 combining this high-quality dataset and the highest-resolution image of the Alpine subduction

256 complex, we demonstrate here that these anomalously deep earthquakes originate in the  
257 shallow mantle. Even under the most conservative tectonic reconstruction of Fig. 3a, the  
258 number of mantle earthquakes recorded along the analyzed cross section since 1990 is >200.

259

## 260 **6.2. Temperature and lithology control on seismicity**

261 The vertical stacking of continental crust and mantle rocks described beneath the Western  
262 Alps provides an excellent framework for testing the role of temperature and lithology on  
263 seismicity. Rocks with contrasting rheological properties are in fact juxtaposed at similar  
264 depths (Fig. 3), and deformation is strongly localized along an active lithospheric strike-slip  
265 fault (Eva et al., 2015). Within this complex lithospheric puzzle, earthquakes are indeed  
266 concentrated in the upper crust, but they are also continuously recorded down to 75 km depth  
267 in the lithospheric mantle beneath the Adriatic Moho, without any major gap with depth. As  
268 shown in Figure 3, most of the earthquakes originate in the continental crust within the  
269 uppermost 15-20 km of the Alpine accretionary wedge, but earthquakes are also observed in  
270 the 20-30 km depth range, either in European lower crust or in mantle rocks not affected by  
271 serpentinization. At depth >30 km, earthquakes are no more observed within the subducted  
272 lower crust, but they are clustered in mantle rocks both in Fig. 3a and in Fig. 3b. Therefore,  
273 our results provide observational evidence that deep material located at the same depth, and  
274 thus at very similar temperature along the same fault, under the same stress conditions can be  
275 seismogenic or not depending on the lithology. In previous work, this kind of analysis was  
276 precluded by insufficient information concerning both the lithospheric structure of the  
277 collision zone, and the localization of deep earthquakes relative to the plate interface.

278 The distribution of earthquake depths observed in the Western Alps confirms the global  
279 view of seismicity (e.g., Priestley et al., 2008; Chen et al., 2013), which states that (i)  
280 earthquakes dominantly occur in upper crust colder than  $\sim 300^{\circ}\text{C}$ , and predicts that (ii)

281 earthquakes might potentially occur in the mantle, if colder than  $\sim 600^{\circ}\text{C}$ . Our results provide  
282 direct evidence confirming this prediction. This general behaviour is ascribed to the onset of  
283 crystal plasticity of quartz in the crust and olivine in the upper mantle, which precludes  
284 frictional instability at higher temperatures (Scholz, 1998; Raterron et al., 2004).  
285 Serpentinization is an additional player possibly favoring aseismic deformation in mantle  
286 rocks (Peacock and Hyndman, 1999; Hilairt et al., 2007), as confirmed by both Figures 3a  
287 and 3b, which show that the anomalously deep earthquakes of the Western Alps chiefly  
288 originate in mantle rocks not affected by serpentinization.

289 Our results thus confirm the major role played by temperature and lithology in controlling  
290 the earthquake distribution with depth. In the light of the low stress inferred from earthquake  
291 magnitudes, this implies that the Adriatic mantle at  $\sim 75$  km depth is colder than  $\sim 600^{\circ}\text{C}$   
292 (e.g., Raterron et al., 2004), which requires geothermal gradients ( $< 8^{\circ}\text{C}/\text{km}$ ) on the order of  
293 those experienced by the European crust during Alpine subduction (Malusà et al., 2015).  
294 Geothermal gradients, on the upper plate side of the Western Alps subduction system, thus  
295 remained very low even after the choking of Alpine subduction, in agreement with the lack of  
296 orogenic magmatism and with the predictions of numerical models (e.g., Jamieson and  
297 Beaumont, 2013). Within the accretionary wedge, by contrast, the relatively low thickness of  
298 the seismogenic layer, and the absence of earthquakes at depth  $> 30$  km, is supportive of an  
299 increase in geothermal gradients after the end of subduction, possibly due to the advection of  
300 heat transported by exhuming (U)HP rocks, as confirmed by independent petrologic and  
301 geochronologic evidence (Malusà et al., 2015). A similar situation is observed north of  
302 eastern Papua New Guinea, where anomalously deep earthquakes are recorded at  $\sim 100$  km  
303 depth (Eilon et al., 2015) on the upper plate side of a chocked subduction zone that brought a  
304 ribbon of Australian continental crust down to (U)HP depth (Baldwin et al., 2012). Like in the

305 Western Alps, these anomalously deep earthquakes have no clear linkage with a subducting  
306 slab.

307

### 308 **6.3. Implications for lithosphere rheology**

309 The rheological properties of the continental lithosphere are an open issue with relevant  
310 implications for a wide range of studies (Burov and Watts, 2006; Bürgmann and Dresen,  
311 2008), and contrasting 1D rheological models have been proposed so far. On the one hand,  
312 the conventional “jelly sandwich” rheological model (Chen and Molnar, 1983; Chen and  
313 Yang, 2004) envisages a weak aseismic lower crust separating two rigid seismogenic layers,  
314 represented by the upper crust and the uppermost mantle. On the other hand, the alternative  
315 “crème brûlée” model (Jackson, 2002; Priestley et al., 2008) envisages a single strong  
316 seismogenic layer that may either involve the upper crust or the whole crust, but does not  
317 include the mantle. These simple end-member models have been applied to orogenic belts  
318 with a relatively constant structure along strike, such as the Himalayas (Chen and Yang, 2004;  
319 Priestley et al., 2008), but they might be more difficult to apply in the case of a complex 3D  
320 structure as expected in the Western Alps.

321 The Western Alps case study shows that major gaps in earthquake distribution with depth,  
322 as predicted by the jelly sandwich model (Chen and Molnar, 1983; Burov and Watts, 2006),  
323 are not necessarily required. Moreover, it demonstrates that the upper mantle can be stiff and  
324 seismogenic not only in cold cratons, as predicted by the crème brûlée model (Priestley et al.,  
325 2008), but also in young orogenic belts.

326

## 327 **7. Conclusions**

328 The combined analysis of lithospheric structure and distribution of anomalously deep  
329 earthquakes in the Western Alps shed new light on the rheological properties of the continental  
330 lithosphere, and led to the following main conclusions:

331 1) The anomalously deep earthquakes of the Western Alps are aligned on an active  
332 lithospheric fault located in the mantle wedge between the European Moho and the  
333 Adriatic Moho. This provides compelling evidence that seismic activity and brittle  
334 faulting can occur in the shallow continental mantle of a young collision zone.

335 2) Earthquakes in the Western Alps are concentrated in the upper crust, but they are also  
336 continuously recorded in the lithospheric mantle down to 75 km depth. No earthquake is  
337 instead observed in the subducted European crust at depth greater than 30 km. This  
338 provides direct evidence that temperature and lithology exert a major role in controlling  
339 earthquake distribution with depth.

340 3) The anomalously deep earthquakes of the Western Alps chiefly originate in mantle  
341 rocks not affected by serpentinization. This confirms the role of serpentinization in  
342 favoring aseismic creep.

343 4) The earthquake distribution with depth observed in the Western Alps shows that the  
344 major seismic gap predicted by the jelly sandwich rheologic model is not necessarily  
345 required, and demonstrates that the mantle of a young continental plate can be stiff and  
346 seismogenic unlike predicted by the crème brûlée model. These findings should be  
347 integrated in future, more realistic rheologic models of the continental lithosphere.

348

#### 349 **Acknowledgments**

350 This work is funded by the State Key Laboratory of Lithospheric Evolution, China, the National  
351 Natural Science Foundation of China (Grant 41350001), and a grant from LabEx OSUG@2020  
352 (Investissements d'avenir; ANR10 LABX56, France). The earthquake waveforms used in this study  
353 are available at the European Integrated Data Archive ([eida.rm.ingv.it](http://eida.rm.ingv.it)) (see also

354 doi:10.13127/SD/X0FXnH7QfY; doi:10.12686/sed/networks/2a). The seismic data used for the  
355 receiver-function imaging are archived at the data center of the Seismic Array Laboratory, Institute of  
356 Geology and Geophysics, Chinese Academy of Sciences, and at the data center of the French  
357 Seismologic and Geodetic Network RESIF (doi:10.15778/RESIF.YP2012). The manuscript benefited  
358 from constructive reviews by W.P. Chen and an anonymous reviewer, and from insightful comments  
359 by S. Baldwin, L. Jolivet and C. Pasquero.

360

## 361 **References**

- 362 Andersen, T. B., Austrheim, H., 2006. Fossil earthquakes recorded by pseudotachylytes in mantle  
363 peridotite from the Alpine subduction complex of Corsica. *Earth and Planetary Science Letters*  
364 242(1), 58-72.
- 365 Baldwin, S. L., Fitzgerald, P. G., Webb, L. E., 2012. Tectonics of the New Guinea region. *Annual*  
366 *Review of Earth and Planetary Sciences* 40, 495–520.
- 367 Bellahsen, N., Mouthereau, F., Boutoux, A., Bellanger, M., Lacombe, O., Jolivet, L., Rolland, Y.,  
368 2014. Collision kinematics in the western external Alps, *Tectonics* 33(6), 1055-1088.
- 369 Bürgmann, R., Dresen, G., 2008. Rheology of the lower crust and upper mantle: Evidence from  
370 rock mechanics, geodesy, and field observations. *Annual Review of Earth and Planetary Sciences*  
371 36, 531–567.
- 372 Burov, E., Watts, A. B., 2006. The long-term strength of continental lithosphere: jelly-sandwich or  
373 crème-brûlée? *GSA Today* 16, 4-10.
- 374 Chen, W. P., Molnar, P., 1983. Focal depths of intracontinental and intraplate earthquakes and  
375 their implication for the thermal and mechanical properties of the lithosphere. *Journal of*  
376 *Geophysical Research* 88, 4183-4214.
- 377 Chen, W. P., Yang Z., 2004. Earthquakes beneath the Himalaya and Tibet: evidence for a strong  
378 lithospheric mantle. *Science* 304, 1949–1952.
- 379 Chen, W. P., Yu, C. Q., Tseng, T. L., Yang, Z., Wang, C. Y., Ning, J., Leonard, T., 2013. Moho,  
380 seismogenesis, and rheology of the lithosphere. *Tectonophysics* 609, 491–503.
- 381 Closs, H., Labrouste, Y. (Eds.), 1963. *Recherches séismologiques dans les Alpes occidentales au*  
382 *moyen de grandes explosions en 1956, 1958 et 1960. Mémoire collectif du Groupe d'études des*  
383 *explosions alpines, Année géophysique internationale 12–2. Centre national de la recherche*  
384 *scientifique, Paris, 241 pp.*
- 385 Delacou, B., Sue, C., Champagnac, J. D., Burkhard, M., 2004. Present-day geodynamics in the  
386 bend of the western and central Alps as constrained by earthquake analysis. *Geophysical Journal*  
387 *International* 158, 753-774.
- 388 Dewey, J.F., Helman, M.L., Turco, E., Hutton, D.H.W., Knott, S.D., 1989. Kinematics of the  
389 western Mediterranean, in: Coward, M.P., Dietrich, D., Park, R.G. (Eds.), *Alpine tectonics*. *Geol.*  
390 *Soc. London Spec. Publ.* 45, pp. 265–283.



- 391 Dumont, T., Schwartz, S., Guillot, S., Simon-Labric, T., Tricart, P., Jourdan, S., 2012. Structural  
392 and sedimentary records of the Oligocene revolution in the Western Alpine arc. *Journal of*  
393 *Geodynamics* 56, 18–38.
- 394 Eilon, Z., Abers, G. A., Gaherty, J. B., Jin, G., 2015. Imaging continental breakup using  
395 teleseismic body waves: The Woodlark Rift, Papua New Guinea. *Geochemistry, Geophysics,*  
396 *Geosystems* 16(8), 2529-2548.
- 397 Eva, E., Solarino, S., 1998. Variations of stress directions in the western Alpine arc. *Geophysical*  
398 *Journal International* 135, 438–448.
- 399 Eva, E., Solarino, S., Eva, C., Neri, G., 1997. Stress tensor orientation derived from fault plane  
400 solutions in the southwestern Alps. *Journal of Geophysical Research* 102(B4), 8171–8185.
- 401 Eva, E., Malusà M. G., Solarino, S., 2015. A seismotectonic picture of the inner southern Western  
402 Alps based on the analysis of anomalously deep earthquakes. *Tectonophysics* 661, 190-199.
- 403 Frohlich, C., Gan, W., Herrmann, R. B., 2015. Two deep earthquakes in Wyoming. *Seismological*  
404 *Research Letters*, 86(3), 810-818.
- 405 Handy, M. R., Schmid, S. M., Bousquet, R., Kissling, E., Bernoulli, D., 2010. Reconciling plate-  
406 tectonic reconstructions of Alpine Tethys with the geological–geophysical record of spreading and  
407 subduction in the Alps. *Earth-Science Reviews* 102, 121–158.
- 408 Hilairret, N., Reynard, B., Wang, Y., Daniel, I., Merkel, S., Nishiyama, N., Petitgirard, S., 2007.  
409 High-pressure creep of serpentine, interseismic deformation, and initiation of subduction. *Science*  
410 318, 1910-1913.
- 411 Inbal, A., Ampuero, J. P., Clayton, R. W., 2016. Localized seismic deformation in the upper  
412 mantle revealed by dense seismic arrays. *Science*, 354(6308), 88-92.
- 413 Jackson, J., 2002. Strength of the continental lithosphere: time to abandon the jelly sandwich?  
414 *GSA Today* 12, 4-9.
- 415 Jamieson, R. A., Beaumont, C., 2013. On the origin of orogens. *Geological Society of America*  
416 *Bulletin* 125(11-12), 1671–1702.
- 417 Jolivet, L., Faccenna, C., Goffé, B., Burov, E., Agard, P., 2003. Subduction tectonics and  
418 exhumation of high-pressure metamorphic rocks in the Mediterranean orogens. *American Journal*  
419 *of Science* 303, 353–409.
- 420 Kufner, S. K., Schurr, B., Sippl, C., Yuan, X., Ratschbacher, L., Mohammad Akbar, A., Ischuk,  
421 A., Murodkulov, S., Schneider, F., Mechie, J., Tilmann, F., 2016. Deep India meets deep Asia:  
422 Lithospheric indentation, delamination and break-off under Pamir and Hindu Kush (Central Asia).  
423 *Earth and Planetary Science Letters* 435, 171-184.
- 424 Lardeaux, J. M., Schwartz, S., Tricart, P., Paul, A., Guillot, S., Béthoux, N., Masson, F., 2006. A  
425 crustal-scale cross-section of the southwestern Alps combining geophysical and geological  
426 imagery. *Terra Nova* 18(6), 412–422.
- 427 Ligorria, J., Ammon, C. J., 1999. Iterative deconvolution and receiver-function estimation.  
428 *Bulletin of the Seismological Society of America* 89, 1395-1400.
- 429 Maggi, A., Jackson, J., McKenzie, D., Priestley, K., 2000a. Earthquake focal depths, effective  
430 elastic thickness, and the strength of the continental lithosphere. *Geology* 28, 495–498.

- 431 Maggi, A., Jackson, J., Priestley, K., Baker, C., 2000b. A re-assessment of focal depth distribution  
432 in southern Iran, the Tien Shan and northern India: do earthquakes really occur in the continental  
433 mantle? *Geophysical Journal International* 143, 629–661.
- 434 Malusà, M. G., Balestrieri, M. L., 2012. Burial and exhumation across the Alps-Appennines  
435 junction zone constrained by fission-track analysis on modern river sands. *Terra Nova* 24, 221–  
436 226.
- 437 Malusà, M. G., Polino, R., Zattin, M., 2009. Strain partitioning in the axial NW Alps since the  
438 Oligocene. *Tectonics* 28, TC3005, doi:10.1029/2008TC002370.
- 439 Malusà, M. G., Faccenna, C., Garzanti, E., Polino, R., 2011. Divergence in subduction zones and  
440 exhumation of high-pressure rocks (Eocene Western Alps). *Earth and Planetary Science Letters*  
441 310, 21–32.
- 442 Malusà, M. G., Faccenna, C., Baldwin, S. L., Fitzgerald, P. G., Rossetti, F., Balestrieri, M. L.,  
443 Danišák, M., Ellero, A., Ottria, G., Piromallo, C., 2015. Contrasting styles of (U)HP rock  
444 exhumation along the Cenozoic Adria-Europe plate boundary (Western Alps, Calabria, Corsica).  
445 *Geochemistry, Geophysics, Geosystems* 16, 1786-1824.
- 446 Molinari, I., Argnani, A., Morelli, A., Basini, P., 2015. Development and testing of a 3D seismic  
447 velocity model of the Po Plain sedimentary basin, Italy. *Bulletin of the Seismological Society of*  
448 *America* 105(2A), 753-764.
- 449 Monsalve, G., Sheehan, A., Schulte-Pelkum, V., Rajaure, S., Pandey, M. R., Wu, F., 2006.  
450 Seismicity and one-dimensional velocity structure of the Himalayan collision zone: earthquakes in  
451 the crust and upper mantle. *Journal of Geophysical Research* 111.B10.
- 452 Mouthereau, F., Watts, A. B., Burov, E., 2013. Structure of orogenic belts controlled by  
453 lithosphere age. *Nature Geoscience* 6, 785-789.
- 454 Negredo, A.M., Replumaz, A., Villaseñor, A., Guillot, S., 2007. Modeling the evolution of  
455 continental subduction processes in the Pamir–Hindu Kush region. *Earth and Planetary Science*  
456 *Letters* 259, 212-225.
- 457 Nicolas, A., Hirn, A., Nicolich, R., Polino, R., 1990. Lithospheric wedging in the western Alps  
458 inferred from the ECORS-CROP traverse. *Geology* 18, 587–590.
- 459 Peacock, S. M., Hyndman, R. D., 1999. Hydrous minerals in the mantle wedge and the maximum  
460 depth of subduction thrust earthquakes. *Geophysical Research Letters* 26(16), 2517-2520.
- 461 Perrone, G., Eva, E., Solarino, S., Cadoppi, P., Balestro, G., Fioraso, G., Tallone, S., 2010.  
462 Seismotectonic investigations in the inner Cottian Alps (Italian Western Alps): An integrated  
463 approach. *Tectonophysics* 496, 1-16.
- 464 Piromallo, C., Faccenna, C., 2004. How deep can we find the traces of Alpine subduction?  
465 *Geophysical Research Letters* 31, L06605, doi:10.1029/2003GL019288
- 466 Priestley, K., Jackson, J., McKenzie, D., 2008. Lithospheric structure and deep earthquakes  
467 beneath India, the Himalaya and southern Tibet. *Geophysical Journal International* 172, 345-362.
- 468 Raterron, P., Wu, Y., Weidner, D. J., Chen, J., 2004. Low-temperature olivine rheology at high  
469 pressure. *Physics of the Earth and Planetary Interiors* 145, 149-159.

470 Reasenber, P. A., Oppenheimer, D., 1985. FPFIT, FPLOT and FPPAGE: FORTRAN Computer  
471 programs for calculating and displaying earthquake fault-plane solutions. United States Geological  
472 Survey Open-File Report 85-739, 1-109.

473 Reynard, B., 2013. Serpentinite in active subduction zones. *Lithos* 178, 171-185.

474 Richards, M. A., Yang, W. S., Baumgardner, J. R., Bunge, H. P., 2001. Role of a low - viscosity  
475 zone in stabilizing plate tectonics: Implications for comparative terrestrial planetology.  
476 *Geochemistry, Geophysics, Geosystems* 2, 1-12.

477 Scafidi, D., Solarino, S., Eva, C., 2009. P wave seismic velocity and Vp/Vs ratio beneath the  
478 Italian Peninsula from local earthquake tomography. *Tectonophysics* 465, 1-23.

479 Scholz, C.H., 1998. Earthquakes and friction laws. *Nature* 391, 37-42.

480 Serpelloni, E., Anzidei, M., Baldi, P., Casula, G., Galvani, A., 2005. Crustal velocity and strain-  
481 rate fields in Italy and surrounding regions: new results from the analysis of permanent and non-  
482 permanent GPS networks. *Geophysical Journal International* 161(3), 861-880.

483 Serpelloni, E., Faccenna, C., Spada, G., Dong, D., Williams, S. D., 2013. Vertical GPS ground  
484 motion rates in the Euro - Mediterranean region: New evidence of velocity gradients at different  
485 spatial scales along the Nubia - Eurasia plate boundary. *Journal of Geophysical Research* 118,  
486 6003-6024.

487 Sue, C., Thouvenot, F., Fréchet, J., Tricart, P., 1999. Widespread extension in the core of the  
488 western Alps revealed by earthquake analysis. *Journal of Geophysical Research* 104, 25611-  
489 25622.

490 Takeuchi, M., Arai, S., 2015. Upper mantle can in-situ fracture: an implication from a cataclastic  
491 peridotite xenolith from Megata, Northeast Japan arc. *Mineralogy and Petrology* 109, 283-294.

492 Thouvenot, F., Paul, A., Frechet, J., Béthoux, N., Jenatton, L., Guiguet, R., 2007. Are there really  
493 superposed Mohos in the southwestern Alps? New seismic data from fan-profiling reflections.  
494 *Geophysical Journal International* 170, 1180-1194.

495 Vauchez, A., Tommasi, A., Mainprice, D., 2012. Faults (shear zones) in the Earth's mantle.  
496 *Tectonophysics* 558-559, 1-27.

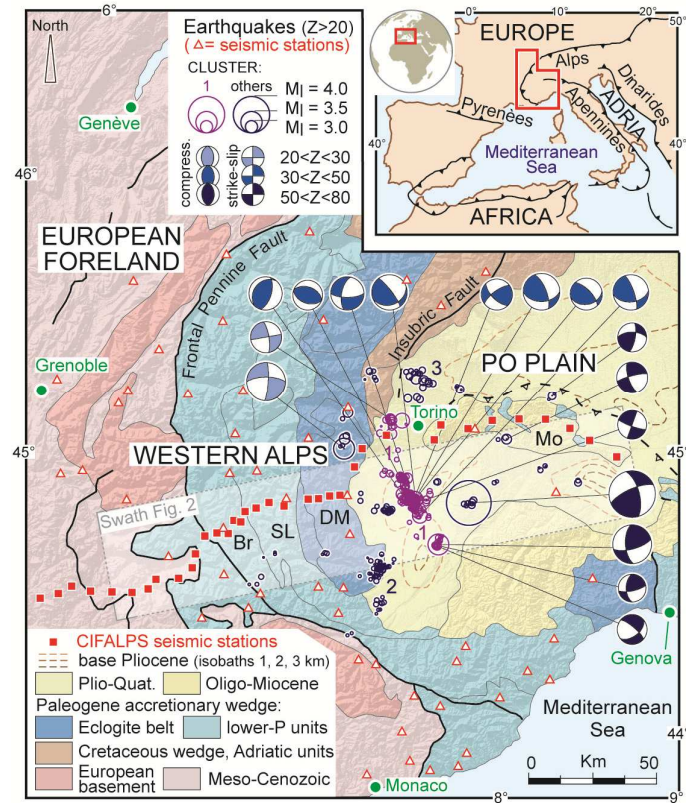
497 Waldhauser, F., Ellsworth, W. L., 2000. A double-difference earthquake location algorithm: method  
498 and application to the northern Hayward fault, California. *Bulletin of the Seismological Society of*  
499 *America* 90, 1353-1368.

500 Zhao, L., Paul, A., Guillot, S., Solarino, S., Malusà, M. G., Zheng, T., Aubert, C., Salimbeni, S.,  
501 Dumont, T., Schwartz, S., Zhu, R., Wang, Q., 2015. First seismic evidence for continental  
502 subduction beneath the Western Alps. *Geology* 43, 815-818.

503 Zhao, L., Paul, A., Malusà, M. G., Xu, X., Zheng, T., Solarino, S., Guillot, S., Schwartz, S.,  
504 Dumont, T., Salimbeni, S., Aubert, C., Pondrelli, S., Wang, Q., Zhu, R., 2016. Continuity of the  
505 Alpine slab unraveled by high-resolution P-wave tomography. *Journal of Geophysical Research*,  
506 doi:10.1002/2016JB013310.

507 Zhu, L., 2000. Crustal structure across the San Andreas Fault, southern California from  
508 teleseismic converted waves. *Earth and Planetary Science Letters* 179, 183-190.

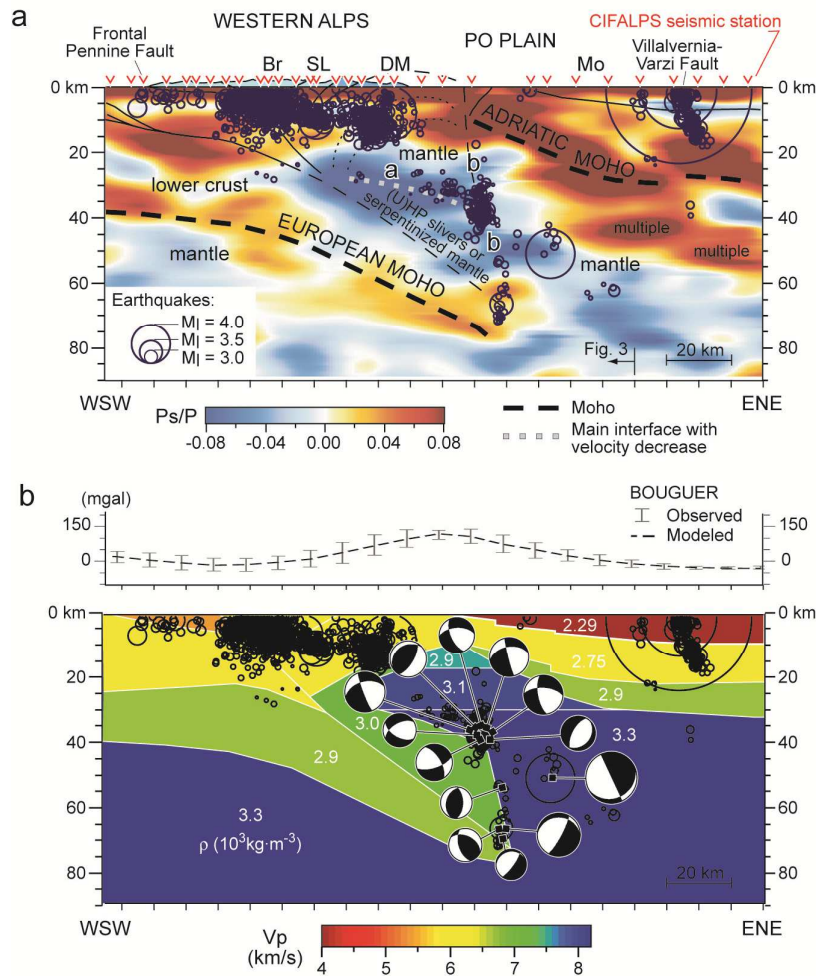
509



510

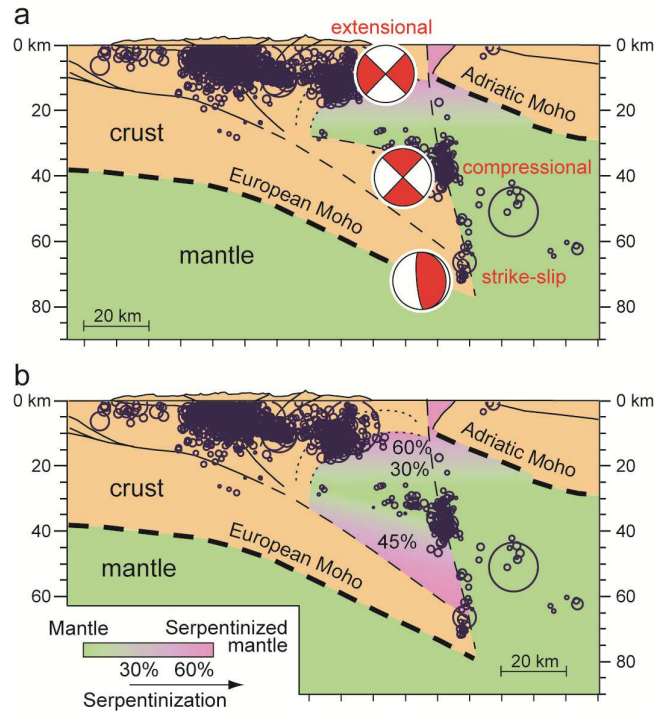
511 **Figure 1: The anomalously deep earthquakes of the Western Alps.** Circles show the  
 512 magnitude ( $M_I$ ) and distribution of all the events, recorded between 1990 and 2014, located at  
 513 depth ( $Z$ )  $> 20$  km ( $n=317$  after HypoDD relocation); beach balls show focal solutions in  
 514 different depth ranges; 1 to 3 indicate earthquake clusters as discussed in the text: cluster 1  
 515 (purple) marks an active lithospheric fault masked by thick Plio-Quaternary sediments. The  
 516 red triangles indicate the network used to record the seismicity, the red squares indicate the  
 517 location of the broadband seismic stations of the CIFALPS experiment (Zhao et al., 2015).  
 518 Abbreviations: Br, Briançonnais; DM, Dora Maira; Mo, Monferrato; SL, Schistes lustrés.

519



520

521 **Figure 2: Relocated earthquakes and seismic imaging combined. a)** Earthquakes within  
 522 the 40-km-thick stripe in Fig. 1 are plotted on the receiver-function cross-section of the  
 523 CIFALPS experiment (Zhao et al., 2015, abbreviations as in Fig. 1). Positive- and negative-  
 524 polarity Ps-converted phases are shown in red and blue, respectively, according to the color  
 525 scale. The dashed black lines indicate the European and Adriatic Mohos, the dashed grey line  
 526 indicates a main interface with velocity decrease; “a” and “b” indicate earthquake alignments  
 527 with different dip angles, as discussed in the text; events located at depth <20 km are also  
 528 included. **b)** Focal solutions for events deeper than 20 km are projected, onto the vertical  
 529 plane, on the 2D velocity and gravity model of the CIFALPS experiment (density values in  
 530 white). Modeled and observed Bouguer gravity anomaly data are also shown (Zhao et al.,  
 531 2015). The largest strike-slip earthquake ( $Z > 50$  km) occurring ~20 km to the east of the  
 532 main alignment “b”, which marks a lithospheric fault, might be also located along a similar  
 533 structure located farther east.



534

535 **Figure 3: Earthquakes in the Western Alps mantle and focal mechanism heterogeneity**  
 536 **with depth.** Frames a and b show two end-member tectonic interpretations, either  
 537 encompassing a thick complex of (U)HP continental slivers (a) or serpentinized mantle (b) on  
 538 top of the slab (the amount of serpentinization is inferred from P-wave velocity - e.g.,  
 539 Reynard, 2013). Shallow earthquakes (<20 km depth) are concentrated in the uplifting  
 540 accretionary wedge, whereas the anomalously deep events (>20 km depth) are concentrated,  
 541 in both models, in the mantle wedge beneath the Adriatic Moho ( $M_1$  scale as in Fig. 2), and in  
 542 mantle rocks not affected by serpentinization. According to the more conservative end-  
 543 member hypothesis of Fig. 3a, more than 200 earthquakes have been recorded in the mantle  
 544 along the analyzed cross section since 1990. Fault plane solutions (summarized by red  
 545 beachballs in frame a) define a vertical stacking of extensional (e.g., Eva and Solarino, 1998),  
 546 compressional and strike-slip events. No seismicity is observed along the European Moho.